Received: 30 December 2017 | Revised: 12 April 2018 | Accepted: 26 April 2018 | Published on: 12 November 2018

DOI: 10.1002/qj.3332

RESEARCH ARTICLE

Quarterly Journal of the Royal Meteorological Society RMetS

The generation of kinetic energy in tropical cyclones revisited

Roger K. Smith[1] | Michael T. Montgomery[2] | Gerard Kilroy[1]

[1]Meteorological Institute, Ludwig Maximilian University of Munich, Munich, Germany
[2]Department of Meteorology, Naval Postgraduate School, Monterey, California

Correspondence
Roger K. Smith, Meteorological Institute, Ludwig-Maximilians University of Munich, Theresienstr. 37, 80333 Munich, Germany.
Email: roger.smith@lmu.de

Many previous diagnoses of the global kinetic energy budget for a tropical cyclone have given prominence to the global integral of a pressure–work term in the generation of kinetic energy. However, in his erudite textbook *Atmosphere–Ocean Dynamics*, Adrian Gill derives a form of the kinetic energy equation in which there is no such explicit source term. In this article we revisit the interpretations of the generation of kinetic energy given previously in light of Gill's analysis and compare the various interpretations, which are non-unique. Further, although global energetics provide a constraint on the flow evolution, in the context of the kinetic energy equation they conceal important aspects of energy generation and consumption, a finding which highlights the limitations of a global kinetic energy budget in revealing the underlying dynamics of tropical cyclones.

KEYWORDS

energetics, hurricane, spin up, tropical cyclone, typhoon

1 | INTRODUCTION

In a classic review paper, Anthes (1974, sect. DI) summarizes the global energetics of tropical cyclones, based in part on the work of Palmén and Jordan (1955) and Palmén and Riehl (1957). In this review he argues that the kinetic energy is dominated by the horizontal velocity components and he derives an expression for the rate of generation of kinetic energy, showing that "the important source of kinetic energy production in the hurricane is the radial flow toward lower pressure in the inflow layer, represented by $u\partial p/\partial r$." (Here u is the radial velocity component, r is the radius and p is the pressure). In a similar vein, Palmén and Riehl (1957) note that "the generation depends on the vertical correlation between radial flow component and pressure gradient which, for production of kinetic energy, must be positive, i.e., the strongest inflow must occur at the strongest inward directed pressure gradient." They conclude that "kinetic energy production within the cyclone can take place only if the cyclone is of the warm core type." Anthes goes on to argue that "this inflow is a result of surface friction, which reduces the tangential wind speed and thereby destroys the gradient balance, so that the inward pressure gradient force exceeds the Coriolis and centripetal forces. In the warm core low the maximum pressure gradient ($\partial p/\partial r < 0$)[1] occurs just above the surface layer, at which the inflow ($u < 0$) is maximum in magnitude. In the outflow layer, where the radial flow is reversed, the pressure gradient is much weaker. The result is a net production of kinetic energy, dominated by the contribution from the inflow region."

The foregoing interpretations seem at odds with the kinetic energy equation in flux form presented by Gill (1982) in which the term $-u\partial p/\partial r$ does not appear. Nevertheless, in the context of tropical cyclones, subsequent work has built on the formulation by Palmén and Riehl as reviewed by Anthes (e.g., Kurihara, 1975; Tuleya and Kurihara, 1975; Frank, 1977; DiMego and Bosart, 1982; Hogsett and Zhang, 2009; Wang *et al.*, 2016). The generation of kinetic energy in the context of the global climate is discussed by Peixoto and Oort (1992, sect. 13.2).

The purpose of this article is to reconcile the different interpretations of kinetic energy generation and to calculate the various terms in the kinetic energy budget from an idealized high-resolution numerical simulation of a tropical cyclone.

[1]Presumably Anthes meant $\partial p/\partial r > 0$.

2 | KINETIC ENERGY EQUATIONS

In its most basic form, the momentum equation may be written as

$$\frac{\partial \mathbf{u}}{\partial t} + \mathbf{u}\cdot\nabla\mathbf{u} + \mathbf{f}\wedge\mathbf{u} = -\frac{1}{\rho}\nabla p - g\mathbf{k} - \mathbf{F}, \tag{1}$$

where $\mathbf{u}$ is the three-dimensional velocity vector, p is the pressure, ρ is the density, $\mathbf{F}$ is the frictional force per unit mass opposing the motion, $\mathbf{f} = f\mathbf{k}$, f is the Coriolis parameter ($2\Omega\sin\phi$, where ϕ is latitude and Ω is the Earth's rotation rate), g is the acceleration due to gravity and $\mathbf{k}$ is the unit vector in the vertical direction (here and below, all vector quantities are in bold type). For simplicity, an f-plane is assumed (f = constant) and the Coriolis terms proportional to the cosine of the latitude have been neglected as is customary for geophysical flow analyses off the Equator (e.g., McWilliams, 2011).

The kinetic energy equation is obtained by taking the scalar product of Equation 1 with $\mathbf{u}$ using the identity $\mathbf{u}\cdot\nabla\mathbf{u} = \nabla(\frac{1}{2}\mathbf{u}^2) + \boldsymbol{\omega}\wedge\mathbf{u}$, where $\boldsymbol{\omega} = \nabla\wedge\mathbf{u}$ is the vorticity vector. This procedure gives

$$\frac{\partial}{\partial t}(\tfrac{1}{2}\mathbf{u}^2) + \mathbf{u}\cdot\nabla(\tfrac{1}{2}\mathbf{u}^2) = -\frac{1}{\rho}\mathbf{u}\cdot\nabla p - gw - \mathbf{u}\cdot\mathbf{F}, \tag{2}$$

where $w = \mathbf{k}\cdot\mathbf{u}$ is the vertical component of velocity. Note that the Coriolis force ($-\mathbf{f}\wedge\mathbf{u}$) does not appear in the energy equation because it is orthogonal to $\mathbf{u}$.

An alternative form of the kinetic energy equation is obtained by removing some hydrostatically balanced reference pressure, $p_{ref}(z)$, from Equation 1, where $dp_{ref}/dz = -g\rho_{ref}$ defines a reference density, ρ_{ref}, that is a function of altitude z. Then, with the substitution $p = p_{ref}(z) + p'$ and $\rho = \rho_{ref}(z) + \rho'$, where p' and ρ' are the perturbation pressure and density, respectively, the first two terms on the right-hand side of Equation 1, $-(1/\rho)\nabla p - g\mathbf{k}$, become $-(1/\rho)\nabla p' + b\mathbf{k}$, where $b = -g(\rho - \rho_{ref})/\rho$ is the buoyancy force of an air parcel per unit mass. Then, Equation 2 becomes

$$\frac{\partial}{\partial t}(\tfrac{1}{2}\mathbf{u}^2) + \mathbf{u}\cdot\nabla(\tfrac{1}{2}\mathbf{u}^2) = -\frac{1}{\rho}\mathbf{u_h}\cdot\nabla_h p' + Pw - \mathbf{u}\cdot\mathbf{F}, \tag{3}$$

where $\mathbf{u_h}$ is the horizontal velocity vector, ∇_h is the horizontal gradient operator and

$$P = -\frac{1}{\rho}\frac{\partial p}{\partial z} - g = -\frac{1}{\rho}\frac{\partial p'}{\partial z} + b \tag{4}$$

is the *net* vertical perturbation gradient force per unit mass. Despite the explicit appearance of p' in the first term on the right-hand side of Equation 3, all the terms in this equation are independent of the reference pressure $p_{ref}(z)$, since, in particular, $\mathbf{u_h}\cdot\nabla_h p_{ref}(z) = 0$. For simplicity, we take $p_{ref}(z)$ and $\rho_{ref}(z)$ to be the ambient pressure and density, respectively, assuming that these are in hydrostatic equilibrium. Then p' vanishes at large distances from the vortex axis.

We examine now the different forms of Equation 3 derived by Anthes (1974), Gill (1982) and others, beginning with a slight modification of Gill's formulation.

2.1 | Modified Gill formulation

In essence, Gill's formulation of the kinetic energy equation is as follows. Using the result that for any scalar field, γ,

$$\rho\frac{D\gamma}{Dt} = \frac{\partial}{\partial t}(\rho\gamma) + \nabla\cdot(\rho\gamma\mathbf{u}), \tag{5}$$

where $D/Dt = \partial/\partial t + \mathbf{u}\cdot\nabla$ is the material derivative (see Gill, 1982, eq. 4.3.6),[2] the material form of Equation 3 times ρ may be written in flux form as

$$\frac{\partial}{\partial t}(\tfrac{1}{2}\rho\mathbf{u}^2) + \nabla\cdot\mathbf{F_{KE}} = p'\nabla_h\cdot\mathbf{u_h} + \rho Pw + \frac{\partial(p'w)}{\partial z} - \rho\mathbf{u}\cdot\mathbf{F}, \tag{6}$$

where

$$\mathbf{F_{KE}} = (p' + \tfrac{1}{2}\rho\mathbf{u}^2)\mathbf{u} \tag{7}$$

is the *mechanical energy flux density vector* (Gill, 1982, cf. eq. 4.6.4).

The global kinetic energy budget can be obtained by integrating Equation 6 over a cylindrical volume of space, V, of radius R and height H centred on the storm and using the boundary conditions that $u = 0$ at $r = 0$, and $w = 0$ at $z = 0$ and $z = H$. Here, we use a cylindrical coordinate system (r, λ, z) centred on the vortex, where r is the radius, λ is the azimuth and z is the height. We denote an average of the quantity χ over the volume V by

$$\overline{[\chi]} = \frac{1}{\pi R^2 H}\int_0^R rdr\int_0^{2\pi} d\lambda\int_0^H \chi dz.$$

Then Equation 6 becomes

MODIFIED GILL FORM

$$\frac{d}{dt}\overline{\left[\tfrac{1}{2}\rho\mathbf{u}^2\right]} = \overline{[p'\nabla_h\cdot\mathbf{u_h}]} + \overline{[\rho Pw]} - F_{KEG} - D, \tag{8}$$

where

$$F_{KEG} = \frac{1}{\pi R^2 H}\int_0^{2\pi} d\lambda\int_0^H \left[u(p' + \tfrac{1}{2}\rho\mathbf{u}^2)\right]_{r=R} dz \tag{9}$$

is the *flux of mechanical energy* through the side boundary $r = R$, and for a Newtonian fluid with constant dynamic viscosity coefficient μ,

$$D = \overline{[\mu\Phi_v]}, \tag{10}$$

where, in cylindrical coordinates,

$$\begin{aligned}\Phi_v = 2&\left[\left(\frac{\partial u}{\partial r}\right)^2 + \left(\frac{1}{r}\frac{\partial v}{\partial\lambda} + \frac{u}{r}\right)^2 + \left(\frac{\partial w}{\partial z}\right)^2\right]\\ &+ \left[r\frac{\partial}{\partial r}\left(\frac{v}{r}\right) + \frac{1}{r}\frac{\partial u}{\partial\lambda}\right]^2 + \left[\frac{1}{r}\frac{\partial w}{\partial\lambda} + \frac{\partial v}{\partial z}\right]^2\\ &+ \left[\frac{\partial u}{\partial z} + \frac{\partial w}{\partial r}\right]^2 - \frac{2}{3}(\nabla\cdot\mathbf{u})^2\end{aligned} \tag{11}$$

[2] If the density refers to that of a moist air parcel consisting of dry air, water vapour and liquid water, the density is conserved only if the liquid water component is suspended in the parcel. In the presence of precipitation, there will be a small source or sink of density associated with the flux divergence of falling precipitation. In what follows, we will ignore the effects of this source/sink term in the kinetic energy budget.

is the dissipation function.[3] Here, v is the tangential wind component.

Since $\nabla_h \cdot \mathbf{u_h}$ is the fractional change in the horizontal area of an air parcel per unit time, the first term on the right-hand side of Equation 8 is the cumulative effect of the kinetic energy generated locally when an air parcel with positive perturbation pressure expands in the horizontal, or when one with a negative perturbation pressure contracts in the horizontal. The second term on the right-hand side of this equation represents the rate of kinetic energy production by air rising in the presence of a positive net vertical perturbation pressure gradient force ($P > 0$) and air sinking in the presence of a negative net vertical perturbation pressure gradient force ($P < 0$). In Gill's original formulation, the net vertical perturbation pressure gradient force term in Equation 8 is replaced by a buoyancy force, which by itself is a non-unique force, and the second term on the right-hand side is replaced by $\nabla \cdot \mathbf{u}$, which is the fractional change in volume of an air parcel. Note that, in Gill's formulation, there is no term corresponding with $u\partial p/\partial r$ (or equivalently $u\partial p'/\partial r$) in Anthes' formulation of the problem, which a number of authors have argued is the key term in generating kinetic energy.

2.2 | Generalized Anthes formulation

As noted above, Anthes reasonably supposes that the vertical velocity makes only a small contribution to the global kinetic energy, and his derivation of the kinetic energy equation is based on the horizontal momentum equations only and the neglect of the contribution from $\frac{1}{2}w^2$ in the kinetic energy. Nevertheless, Anthes retains the vertical velocity component in the advection term $\mathbf{u} \cdot \nabla \mathbf{u}$ in Equation 1 and $\mathbf{u} \cdot \nabla(\frac{1}{2}\mathbf{u^2})$ in Equation 2. A slightly generalized form of Anthes' equation follows directly from ρ times Equation 3, which in flux form analogous to Equation 6 is

$$\frac{\partial}{\partial t}(\tfrac{1}{2}\rho\mathbf{u^2}) + \nabla \cdot \mathbf{F_{KEA}} = -\mathbf{u_h} \cdot \nabla_h p' + \rho P w - \rho \mathbf{u} \cdot \mathbf{F}, \qquad (12)$$

where

$$\mathbf{F_{KEA}} = (\tfrac{1}{2}\rho\mathbf{u^2})\mathbf{u}. \qquad (13)$$

Again integrating over the cylinder, Equation 12 becomes

GENERALIZED ANTHES FORM

$$\frac{d}{dt}\overline{\left[\tfrac{1}{2}\rho\mathbf{u^2}\right]} = -\overline{\left[\mathbf{u_h} \cdot \nabla_h p'\right]} + \overline{[\rho P w]} - F_{KEA} - D, \quad (14)$$

where

$$F_{KEA} = \frac{1}{\pi R^2 H}\int_0^{2\pi} d\lambda \int_0^H \left[u(\tfrac{1}{2}\rho\mathbf{u^2})\right]_{r=R} dz. \qquad (15)$$

Equation 14 is a generalization of Anthes' formulation to include the three-dimensional wind vector in the definition of kinetic energy and the rate of working of the net vertical perturbation gradient force per unit volume, $\overline{[\rho P w]}$, which is a non-hydrostatic effect. As in Anthes' original form, the pressure–work term, $-\overline{\left[\mathbf{u_h} \cdot \nabla_h p'\right]}$, appears explicitly in the global form of the kinetic energy equation. For an axisymmetric flow, this term is simply $\overline{\left[-u\partial p/\partial r\right]}$ and, at first sight, one might question its prominence as a source of kinetic energy, since $\partial p/\partial r$ is *not* the only radial force acting on fluid parcels en route to the storm core. Above the frictional boundary layer, the radial pressure gradient is closely balanced by the sum of the centrifugal force and the radial component of the Coriolis force. Moreover, this source term does not appear in Gill's formulation (cf. Equation 8), although it is replaced by the term $\overline{\left[p'\nabla_h \cdot \mathbf{u_h}\right]}$ and the boundary flux terms are different. Even so, one should bear in mind that even in the axisymmetric case, $\overline{\left[-u\partial p/\partial r\right]}$ is generating *not only a radial contribution to the kinetic energy, but also an azimuthal contribution* through the action of the generalized Coriolis force $-(f + v/r)u$. The generation of this azimuthal contribution is implicit in the kinetic energy equation as the generalized Coriolis force does no work, but this force component does convert radial momentum to tangential momentum.

3 | KINETIC ENERGY BUDGET FOR AN IDEALIZED SIMULATION

We examine now the generation terms in the two forms of the kinetic energy equation for the case of an idealized tropical cyclone simulation. We begin with a brief description of the numerical model and go on to present the results.

3.1 | The numerical model

The numerical model used for this study is Bryan's three-dimensional, non-hydrostatic cloud model (CM1), version 16 (Bryan and Fritsch, 2002). The simulations relate to the prototype problem for tropical cyclone intensification, which considers the evolution of an initially axisymmetric, cloud-free, warm-cored, baroclinic vortex in a quiescent environment on an f-plane. The initial vortex is in thermal wind balance. A latitude of 20°N and a constant sea surface temperature of 28 °C are assumed. The model configuration is

[3]Equation 8 is, in essence, the kinetic energy equation for the Reynolds-averaged flow in which the quantity μ is a turbulent eddy counterpart. In this case, we are presuming that a K-theory closure is adequate so that the Reynolds-averaged equations look essentially like the Newtonian fluid formulation. Further, in the mechanical energy flux through the side boundary in Equation 9 we have neglected the eddy diffusive radial flux of kinetic energy. Relative to the advective flux of kinetic energy, the diffusive flux scales with the inverse Reynolds number of the flow, which is always small compared to unity outside of the surface layer. This conclusion is based on recently obtained estimates of the turbulent eddy diffusivity observed in major hurricanes on the order of 50–100 m^2/s (Zhang *et al.*, 2011)

more or less the same as described in sect. 2 of Črnivec *et al.* (2016). The differences are that, following the work of Mapes and Zuidema (1996), a more realistic time-scale for Newtonian relaxation to the temperature field (10 days) is applied here instead of the previous default value in CM1 (12 hr). Further, an open boundary condition is taken at lateral boundaries instead of rigid walls and the Dunion moist tropical sounding is used as the environmental sounding (Dunion, 2011).

The initial tangential wind speed has a maximum of 15 m/s at the surface at a radius of 100 km. The tangential wind speed decreases sinusoidally with height, becoming zero at a height of 20 km. Above this height, up to 25 km, the tangential wind is set to zero. The balanced pressure, density and temperature fields consistent with this prescribed tangential wind distribution are obtained using the method described by Smith (2006). The calculations are carried out for a period of 4 days with data output every 15 min.

3.2 | A few details of the simulation

Figure 1 summarizes the vortex evolution in the simulation. Figure 1a shows the time series of the maximum azimuthally averaged tangential wind speed, V_{max}, and Figure 1b shows the radius R_{vmax} at which V_{max} occurs. Typically, V_{max} is located a few hundred metres above the surface, within a shallow inflow layer. The evolution is broadly similar to that described in Kilroy *et al.* (2016), who used a different numerical model and a much coarser horizontal resolution (with horizontal grid spacing of 5 km compared with the 1 km used here). In brief, after a gestation period of about a day, during which deep convection becomes established inside R_{vmax}, the vortex undergoes a rapid intensification phase lasting about 36 hr, before reaching a quasi-steady state. Initially R_{vmax} is located at a radius of 100 km, but contracts to a little over 20 km after about 2.25 days. The most rapid contraction occurs during the rapid intensification phase as absolute angular momentum surfaces are drawn inwards quickly within and above the boundary layer.

Figure 1c shows the outermost radius of gale-force winds, R_{gales}, defined here as the radius of 17 m/s azimuthally averaged tangential winds at a height of 1 km, which is approximately at the top of the frictional boundary layer. Shown also is R_{galesF}, defined as the (outer) radius at which the total wind speed at any grid point at a height of 10 m is 17 m/s. Both quantities serve as a measure of the vortex size, R_{galesF} being closest to the quantity used by forecasters,[4] but R_{gales} being the preferred measure from a theoretical viewpoint (Kilroy *et al.*, 2016). The evolution of storm size based on R_{galesF} is similar to that based on R_{gales}, although R_{gales} always exceeds the value of R_{galesF}. After 4 days, R_{gales} exceeds R_{galesF} by about 80 km.

[4]Based on the wind speed in a particular sector and not azimuthally averaged.

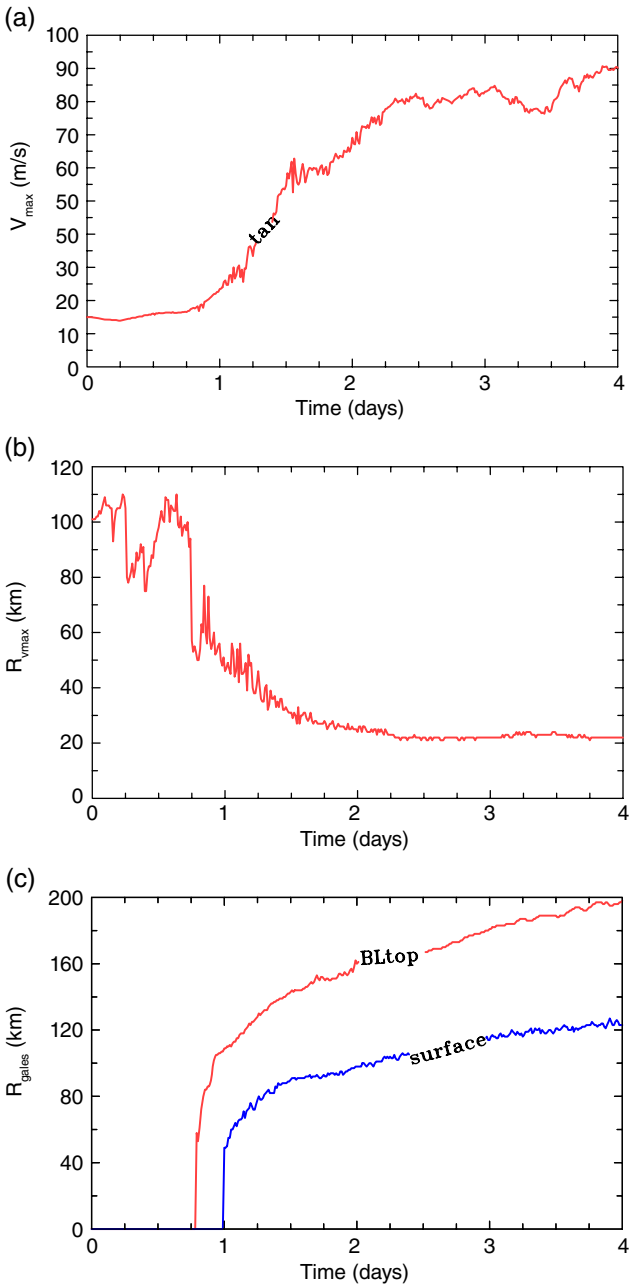

FIGURE 1 (a) Time series of maximum azimuthally averaged tangential wind speed (V_{max}). Panel (b) shows the radius R_{vmax} at which the maximum tangential wind speed occurs. Panel (c) shows the outermost radius of gale force winds (17m/s): "BLtop" refers to the outermost radius at which the azimuthally averaged tangential wind at a height of 1 km equals gale force (R_{gales}) and "surface" refers to the outermost radius where the azimuthally averaged *total* wind equals gale force at a nominal height of 10 m (R_{galesF}) [Colour figure can be viewed at wileyonlinelibrary.com]

Figure 2 shows vertical cross-sections of the azimuthally averaged, 3-hr time-averaged radial and tangential velocity components, the vertical velocity component and the M-surfaces during the intensification phase of the vortex. The time averages are centred on 36 hr during the period of rapid intensification and at 60 hr near the end of this period. The basic features of the flow are qualitatively similar at both times, but all three velocity components strengthen over the period, the M-surfaces move inwards in the lower troposphere

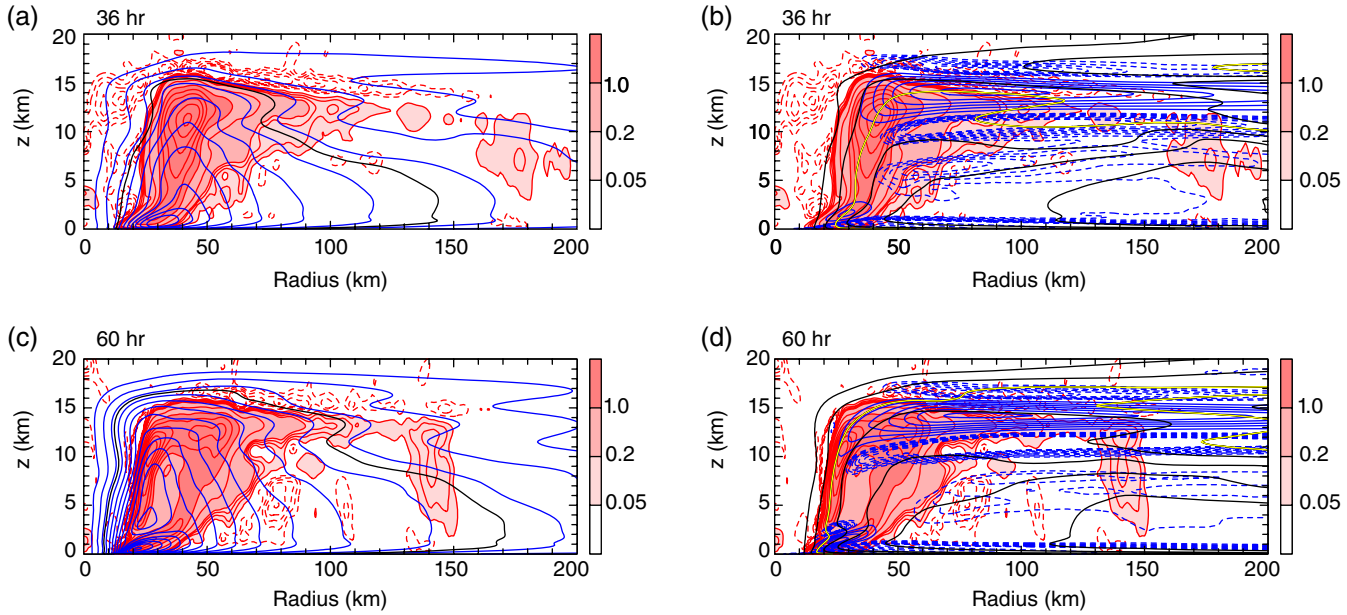

FIGURE 2 (a,c) Vertical cross-sections of the azimuthally averaged, 3-hr time-averaged tangential velocity component (blue contours) centred at 36 and 60 hr. Superimposed are contours and shading of the averaged vertical velocity. Contour intervals are as follows. Tangential velocity: blue contours every 5 m/s, with a thick black contour highlighting the 17 m/s contour. Vertical velocity: thin red contours every 0.05–0.2 m/s; thick red contours at intervals of 0.5 m/s; thin dashed red contours indicating subsidence at intervals of 0.02 m/s. (b,d) Vertical cross-sections of the azimuthally averaged, 3-hr time-averaged radial velocity component, together with the averaged vertical velocity centred at the same times. Contour intervals are as follows. Radial velocity: thick blue contours every 4 m/s (dashed negative); thin blue dashed contours every 0.5 m/s down to −3.5 m/s. Absolute angular momentum: black contours every 2×10^5 m^2/s, with the 6×10^5 m^2/s contour highlighted in yellow [Colour figure can be viewed at wileyonlinelibrary.com]

and outwards in the upper troposphere. The flow structure is similar to that described in many previous studies (see, e.g., the recent review by Montgomery and Smith, 2017a and references therein), with a layer of strong shallow inflow marking the frictional boundary layer, a layer of weaker inflow in the lower troposphere, a region of strong outflow in the upper troposphere and a layer of enhanced inflow below the outflow. The maximum tangential wind speed occurs within, but near the top of the frictional boundary layer.[5] Much of the ascent occurs in an annular region on the order of 50–60 km in radius. The region inside this annulus shows mostly descent.

3.3 | Kinetic energy evolution

Figure 3 shows time series of the domain-averaged kinetic energy per unit volume, $\overline{\left[\frac{1}{2}\rho\mathbf{u}^2\right]}$, for domain radii of 300 and 500 km and a domain height of 20 km. As anticipated by Anthes (1974), this quantity is dominated by the horizontal velocity components; in fact, the curves for $\overline{\left[\frac{1}{2}\rho\mathbf{u}^2\right]}$ and $\overline{\left[\frac{1}{2}\rho\mathbf{u}_\mathbf{h}^2\right]}$ essentially overlap. It follows that the contribution of the vertical velocity to the global kinetic energy is negligible.

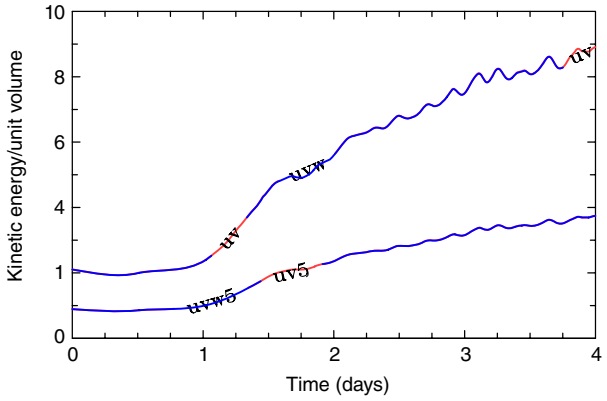

FIGURE 3 Time series of the left-hand side of Equation 14, $\overline{\left[\frac{1}{2}\rho\mathbf{u}^2\right]}$ (curves labelled uvw) compared to $\overline{\left[\frac{1}{2}\rho\mathbf{u}_\mathbf{h}^2\right]}$ (curves labelled uv) for cylinders of 300 and 500 km. The curves for each cylinder size essentially lie on top of each other so that only a single curve is evident. The curves for the 500 km domain are labelled with a "5". Units 10^{-3} W/m^3 [Colour figure can be viewed at wileyonlinelibrary.com]

Notable features of the curves for both domain sizes are the slight decrease during the first 12 hr on account of surface friction, followed by a rapid increase as the vortex intensifies. As time proceeds, the rate of increase progressively declines.

3.4 | Kinetic energy generation: Anthes' formulation

Figure 4 shows time series of the principal terms in the generalized Anthes formulation (the right-hand side of Equation 14), excluding only the global dissipation term since

[5] At 60 hr, the tangential wind field exhibits a second local maximum in the eyewall. This is a transient feature that is presumably associated with a centrifugal wave near the base of the eyewall (e.g., Montgomery and Smith, 2017, p. 550) excited by an elevated pulse of boundary layer outflow shortly before. This feature is not seen at 48 or 72 hr and its presence does not alter the findings concerning the kinetic energy budget.

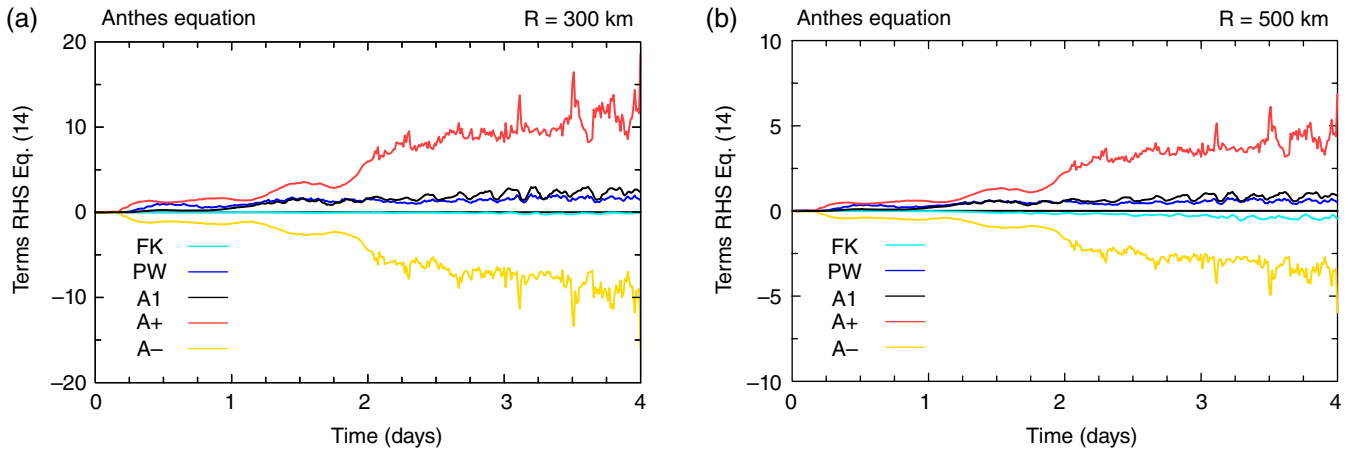

FIGURE 4 Time series of the kinetic energy tendency terms on the right-hand side of Equation 14, the Anthes formulation, averaged over a cylinder of size (a) 300 km and (b) 500 km. Units on the ordinate are 10^{-3} W/m^3. The dissipation term is not shown. A1 stands for $\overline{[-\mathbf{u_h}\cdot\nabla_h p']}$, FK for F_{KEA} and PW for $\overline{[\rho Pw]}$. A1+ and A1− stand for the contributions to A1 from regions where the argument $-\mathbf{u_h}\cdot\nabla_h p'$ is positive and negative, respectively (Note that small values of the generation terms arise because high values of kinetic energy generation are highly localized to the high wind region of the vortex and the averaging volume is large.) [Colour figure can be viewed at wileyonlinelibrary.com]

the focus of the paper is on kinetic energy generation. For both domain radii, 300 km (Figure 4a) and 500 km (Figure 4b), both the terms $\overline{[-\mathbf{u_h}\cdot\nabla_h p']}$ and $\overline{[\rho Pw]}$ are positive, but, perhaps surprisingly, the former term is not appreciably larger than the latter, even beyond 2 days when the differences are largest. The lateral boundary flux term F_{KEA} is virtually zero throughout the calculation. For the larger domain size (R = 500 km), the temporal behaviour of the various terms is similar, but, as expected, the magnitudes of the respective terms are appreciably smaller (Figure 4b), since the largest contributions to the averages are from well inside a 300 km radius (note the different scales on the ordinate in Figure 4a,b).

The finding that the two terms $\overline{[-\mathbf{u_h}\cdot\nabla_h p']}$ and $\overline{[\rho Pw]}$ are not appreciably different in magnitude is at first surprising since, as shown in Figure 3, the contribution of the vertical velocity to the total kinetic energy is negligible. Moreover, the $\overline{[\rho Pw]}$ term does not appear in Anthes' original formulation because the formulation was based on the horizontal momentum equations only. An explanation of this result is suggested by examination of the radius–height structure of the azimuthally averaged generation term before completing the columnar average, i.e. $\langle -\mathbf{u_h}\cdot\nabla_h p'\rangle$, where the angle brackets denote an azimuthal average. The structure of this average together with those of the other generation term, $\langle\rho Pw\rangle$, at 36 and 60 hr, is shown in Figure 5. At both times, the Anthes generation term $\langle -\mathbf{u_h}\cdot\nabla_h p'\rangle$ shows coherent regions of large kinetic energy generation and large kinetic energy destruction. The main region of generation in Figure 5a,b is at low levels, below about 2 km, where the strongest inflow occurs and where the inward directed radial pressure gradient force is particularly strong (Figure 5c,d). There is a second region of generation in an annular column, mostly on the outer side of the eyewall updraught below about 9 km at 36 hr and below about 12 km at 60 hr. The generation terms in Figure 5a,b are similar in structure and magnitude to those shown in fig. 42 (upper right) of Kurihara (1975), for a lower-resolution axisymmetric simulation.

Since the radial pressure gradient is positive at all heights (Figure 5c,d), these generation regions must be ones in which there is generally inflow.[6] For the same reason, where there is outflow, there is kinetic energy removal as seen in the two principal coherent regions in Figure 5a,b where $\langle -\mathbf{u_h}\cdot\nabla_h p'\rangle < 0$. It follows that the computed value of $\overline{[-\mathbf{u_h}\cdot\nabla_h p']}$ is the remainder resulting from the cancellation of two comparatively large contributions from $\langle \mathbf{u_h}\cdot\nabla_h p'\rangle$ of opposite sign, namely $\langle -\mathbf{u_h}\cdot\nabla_h p'\rangle_+$ and $\langle -\mathbf{u_h}\cdot\nabla_h p'\rangle_-$, the former being the sum of all positive values of $-\mathbf{u_h}\cdot\nabla_h p'$ and the latter being the sum of all negative values. This large cancellation is evident in the time series shown in Figure 4.

In summary, a substantial fraction of the kinetic energy that is generated is removed in regions where there is outflow and the residual is relatively small, which is indeed comparable to the kinetic energy generated by the rate of working of the net vertical perturbation pressure gradient force (buoyancy plus perturbation pressure gradient), principally in the region of diabatically forced ascent. The structure of the net vertical perturbation pressure gradient force at 36 and 60 hr is shown in Figure 5e,f. As expected, this force is concentrated in an annular region overlapping the region of diabatic heating.

3.5 | Kinetic energy generation: Gill's formulation

Figures 6a,b show time series of the principal terms in the modified Gill formulation (the right-hand side of Equation 8) for cylinders of 300 km and 500 km radius, again excluding the global dissipation term. In this formulation, the term $\overline{[p'\nabla_h\cdot\mathbf{u_h}]}$ is positive with mean amplitude and fluctuations about this mean increasing with time during the 4 day calculation. For the first day, the term is a little less than the

[6] Note that eddy effects are included in all generation terms.

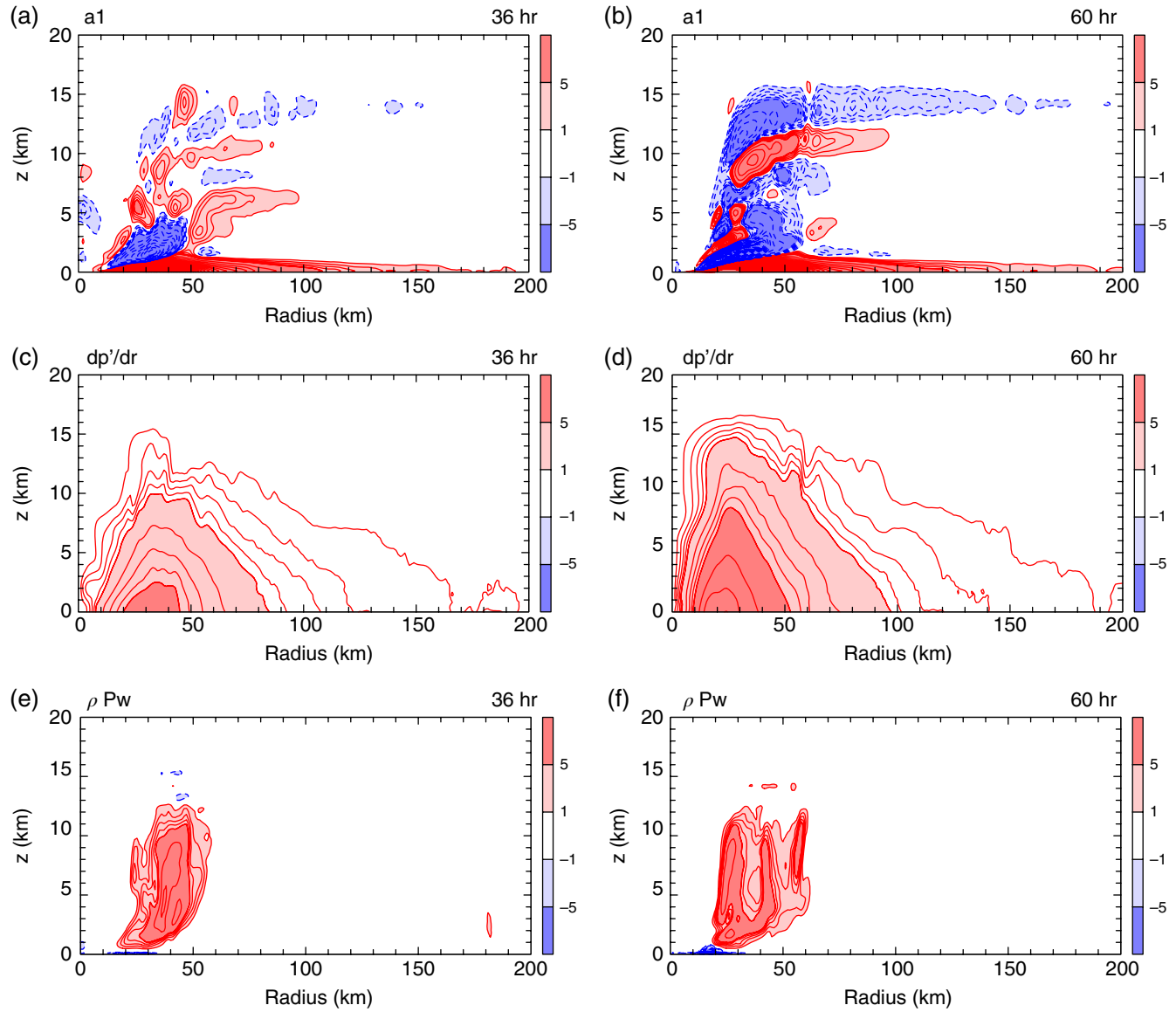

FIGURE 5 Radius–height cross-sections of azimuthally averaged quantities in Equation 14 before performing the columnar average: $\langle -\mathbf{u_h} \cdot \nabla_h p' \rangle$ (a,b) and $\langle \rho Pw \rangle$ (e,f), at 36 hr (left panels) and 60 hr (right panels). Similar cross-sections of $\langle \partial p' / \partial r \rangle$ are shown in (c,d) for these times. Contour intervals are as follows: (a,b,e,f) thick contours 5×10^{-2} W/m^3; thin contours 1×10^{-2} W/m^3; solid red contours positive; dashed blue contours negative; (c,d) thin contours 0.2×10^{-2} Pa/m to 0.8×10^{-2} Pa/m; medium thick contours 1.0×10^{-2} Pa/m to 5.0×10^{-2} Pa/m; thick contours every 5.0×10^{-2} Pa/m. Numbers indicated on the sidebars should be multiplied by 10^{-2} [Colour figure can be viewed at wileyonlinelibrary.com]

$\overline{[\rho Pw]}$ term, but thereafter becomes progressively larger. The increasing energy source represented by the sum of the two foregoing terms is opposed in part by the net outward flux of mechanical energy through the radial boundary, F_{KEG}.

Figure 6c,d shows the structure of the term $\langle p' \nabla_h \cdot \mathbf{u_h} \rangle$, again at 36 and 60 hr. The radial and vertical integrals of this term form the cylindrical average $\overline{[p' \nabla_h \cdot \mathbf{u_h}]}$ in the modified Gill formulation of the energy equation. The qualitative radius–height structure of $\langle p' \nabla_h \cdot \mathbf{u_h} \rangle$ at the two times shown is less easy to infer from the solutions in Figure 2. Moreover, as shown in Figure 6, there is significant cancellation between the term $\overline{[p' \nabla_h \cdot \mathbf{u_h}]}$ and the boundary flux term in Gill's formulation (Equation 8). For this reason, Anthes' formulation of the energy equation would seem to be preferable to Gill's formulation, even though both formulations are correct and give the same tendency of kinetic energy over the control volume of integration (see the next subsection).

3.6 | Total kinetic energy generation

A check on the foregoing calculations is provided by calculating the total tendency of kinetic energy generation, which is the sum of all the terms on the right-hand side of Equations 8 or 14. This sum should be the same for each formulation. That this is the case is verified in Figure 7, which shows the sum for each domain size. As expected, the curves for the two formulations are coincident.

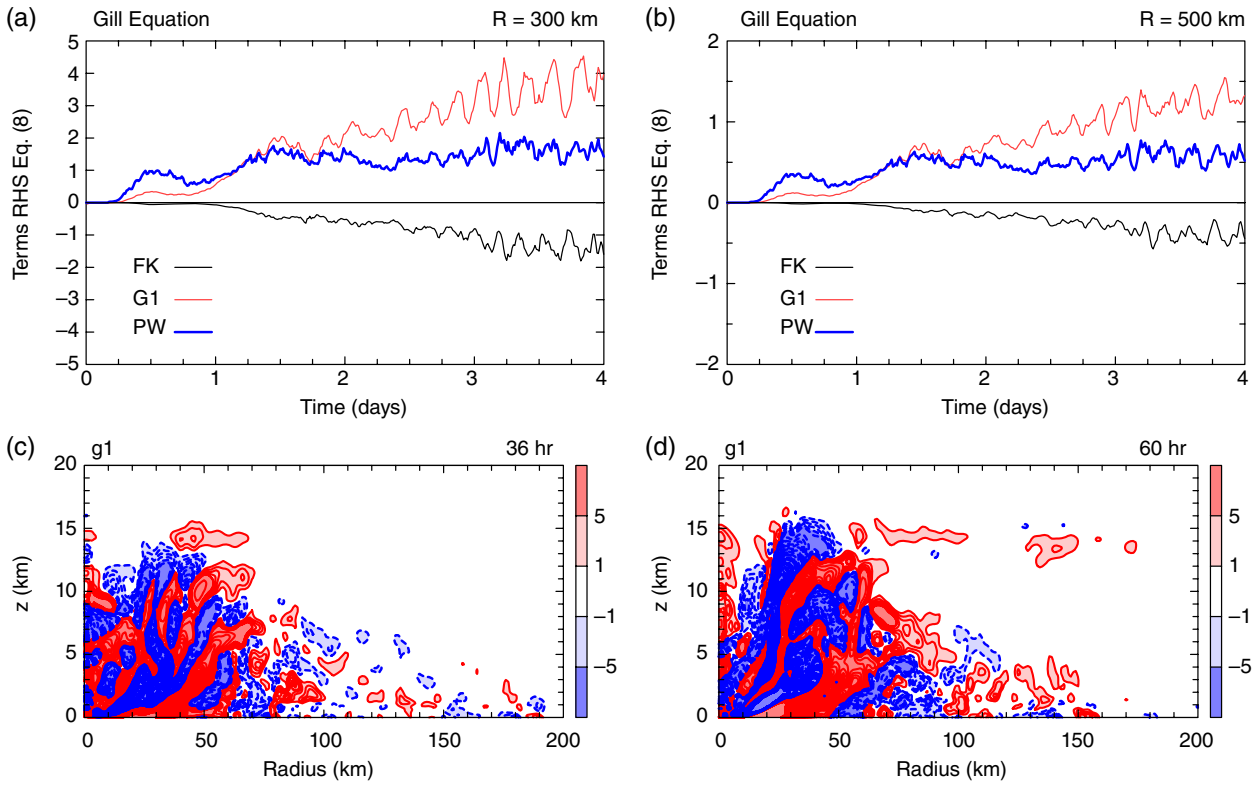

FIGURE 6 Time series of the kinetic energy tendency terms: $\overline{[p'\nabla_h \cdot \mathbf{u_h}]}$ (denoted by G1); $\overline{[\rho Pw]}$ (denoted by PW) and F_{KEG} (denoted by FK) in the modified Gill formulation (Equation 8 averaged over a cylinder of size (a) 300 km and (b) 500 km). Units on the ordinate are 10^{-3} W/m^3. (c,d) The azimuthally averaged terms $\langle p'\nabla_h \cdot \mathbf{u_h} \rangle$ in Equation 8 at 36 and 60 hr, respectively. Contour intervals are as follows: thick contours 5×10^{-2} W/m^3; thin contours 1×10^{-2} W/m^3; solid red contours positive; dashed blue contours negative. Numbers indicated on the sidebars should be multiplied by 10^{-2} [Colour figure can be viewed at wileyonlinelibrary.com]

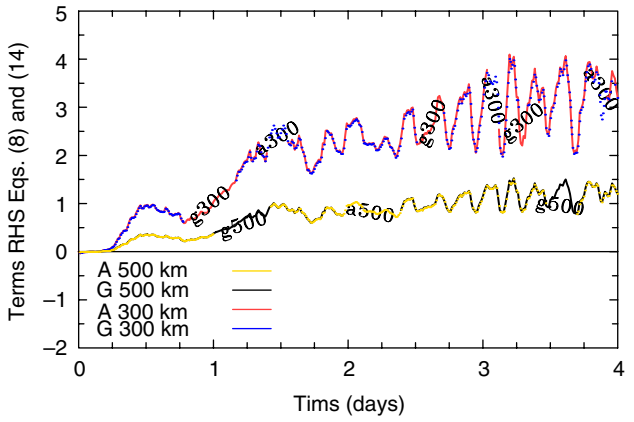

FIGURE 7 Sum of the energy generation terms for Gill's and Anthes' formulations, excluding the dissipation term for cylinders of radius $R = 300$ and 500 km. Values on the ordinate have been multiplied by 10^3 for plotting purposes. The two curves for each value of R essentially lie on top of each other [Colour figure can be viewed at wileyonlinelibrary.com]

4 | DISCUSSION

Anthes' statement noted in the introduction that "the important source of kinetic energy production in the hurricane is the radial flow toward lower pressure in the inflow layer, represented by $-u\partial p/\partial r$" may seem problematic at first because, above the boundary layer, the radial pressure gradient is very closely in balance with the sum of the centrifugal and Coriolis forces. Thus the energy source associated with $-u\partial p/\partial r$ might appear, at least at first, to be a gross overestimate. However, the kinetic energy equation does not recognize the balance constraint and, in this equation, the radial pressure gradient acts to generate not only kinetic energy of radial motion, but also that of tangential motion through the action of the generalized Coriolis force $(f+v/r)u$, a term that appears in the tangential momentum equation in cylindrical coordinates. This is despite the fact that the generalized Coriolis force does not appear explicitly in the kinetic energy equation.

As noted also in the introduction, Anthes recognized that much of the inflow into the storm is "a result of surface friction, which reduces the tangential wind speed and thereby destroys the gradient balance, so that the inward pressure gradient force exceeds the Coriolis and centripetal[7] forces"; he points out also that "in the warm core low the maximum pressure gradient ($-\partial p/\partial r < 0$ [sign corrected: our insertion]) occurs at the lowest level, at which the inflow ($u < 0$) is maximum. In the outflow layer, where the radial flow is reversed, the pressure gradient is much weaker. The result is a net production of kinetic energy, dominated by the contribution from the inflow region." While this view is broadly

[7]Presumably, Anthes means the centrifugal force.

supported by the calculations presented herein, the calculations provide a sharper view of the *net* production of kinetic energy, indicating a region of significant kinetic energy generation accompanying inflow *throughout* the lower troposphere above the boundary layer, as well as significant regions where kinetic energy is consumed as air flows outwards, against the radial pressure gradient force, above the boundary layer. Indeed, the generation above the boundary layer is a manifestation of spin up by the classical mechanism articulated by Ooyama (1969), while the generation within the boundary layer, highlighted by Anthes, is a manifestation of the nonlinear boundary layer spin up mechanism articulated by Smith and Vogl (2008), Smith *et al.* (2009), Smith and Montgomery (2016) and Montgomery and Smith (2017b).

Anthes argues that the boundary layer "must be responsible for a net gain of kinetic energy" even though "a substantial dissipation of kinetic energy in the hurricane occurs in the boundary layer through turbulent diffusion and ultimate loss of energy to the sea surface." As a result, he is led to the paradox that "surface friction is responsible for a net increase in kinetic energy and without friction the hurricane could not exist." The resolution of this paradox would appear to be Anthes' de-emphasis of the role of the classical mechanism for spin up in the kinetic energy budget.

The results of our study, especially the noted cancellation of relatively large generation and consumption contributions to the term $\overline{\left[-\mathbf{u_h}\cdot\nabla_h p'\right]}$, point to limitations in the utility of a global kinetic energy budget in revealing the underlying dynamics of tropical cyclone intensification. An alternative approach would be to examine the energetics of individual air parcels as they move around some hypothetical circuit (see Emanuel (2004) and references therein), but this approach relies on assumptions about the circuits traversed, which may or may not be realizable in reality.

5 | CONCLUSIONS

We have re-examined the traditional theory for kinetic energy generation in a tropical cyclone used by Palmén and Jordan (1955), Palmén and Riehl (1957), Frank (1977) and Hogsett and Zhang (2009), and succinctly summarized in the review article by Anthes (1974). We have compared this with an alternative interpretation of global kinetic energy generation in geophysical flows inspired by Gill (1982), noting that such interpretations are non-unique.

We have shown that the *net* rate of production of kinetic energy is a comparatively small difference between the generation in regions of inflow and the magnitude of the consumption in regions of outflow, so much so that this difference is comparable in magnitude with the rate of generation by the net vertical perturbation pressure gradient force. The latter effect was not contained in Anthes' original formulation, which was based only on the horizontal momentum equations.

We pointed out that the kinetic energy generation term in Anthes' formulation involving the radial pressure gradient does not appear in Gill's formulation of the kinetic energy equation nor in our modification thereof. It is replaced by a term comprising the global integral of the rate of working by perturbation pressure ($\overline{\left[p'\nabla_h\cdot\mathbf{u_h}\right]}$) as the flow expands in the horizontal. However, this generation term is largely compensated in the modified Gill formulation by the boundary flux of mechanical energy (F_{KEG}). The fact that the boundary flux of kinetic energy in the Anthes formulation (F_{KEA}) is typically negligible, as well as the difficulty in anticipating the structure of the term $\overline{\left[p'\nabla_h\cdot\mathbf{u_h}\right]}$ in a tropical cyclone are factors weighing in favour of using Anthes' formulation when applied to the generation of kinetic energy in a tropical cyclone. However, in light of the large cancellation of positive and negative values in the radial pressure–work term, the contribution from the rate of working of the net vertical force is non-negligible in comparison and should be included in any global kinetic energy budget.

While global energetics provide a constraint on flow evolution, we have shown in the context of the kinetic energy equation that they conceal important aspects of energy generation and consumption. This finding highlights the limitations of a global kinetic energy budget in revealing the underlying dynamics of tropical cyclones.

ACKNOWLEDGEMENTS

We thank Dr. Chris Landsea, Dr. Anastassia Makarieva and an anonymous reviewer for their perceptive comments on the original manuscript. GK and RKS acknowledge financial support for tropical cyclone research from the Office of Naval Research Global under Grant No. N62909-15-1-N021. MTM acknowledges the support of NSF grant AGS-1313948, NOAA HFIP grant N0017315WR00048, NASA grant NNG11PK021, ONR grant N0001417WX00336, and the U.S. Naval Postgraduate School.

ORCID

Roger K. Smith https://orcid.org/0000-0002-3668-1608
Michael T. Montgomery https://orcid.org/0000-0001-5383-4648

REFERENCES

Anthes, R.A. (1974) The dynamics and energetics of mature tropical cyclones. *Reviews of Geophysics and Space Physics*, 12, 495–522.

Bryan, G.H. and Fritsch, J.M. (2002) A benchmark simulation for moist nonhydrostatic numerical models. *Monthly Weather Review*, 130, 2917–2928.

Črnivec N, Smith, R.K. and Kilroy, G. (2016) Dependence of tropical cyclone intensification rate on sea-surface temperature. *Quarterly Journal of the Royal Meteorological Society*, 142, 1618–1627.

DiMego, G.J. and Bosart, L.F. (1982) The transformation of tropical storm Agnes into an extratropical cyclone. Part II: moisture, vorticity and kinetic energy budgets. *Monthly Weather Review*, 110, 412–433.

Dunion, J.P. (2011) Rewriting the climatology of the tropical North Atlantic and Caribbean Sea atmosphere. *Journal of Climate*, 24, 893–908.

Emanuel, K. (2004) Tropical cyclone energetics and structure. In: Fedorovich, E., Rotunno, R. and Stevens, B. (Eds.) *Atmospheric Turbulence and Mesoscale Meteorology*. Cambridge: Cambridge University Press, pp. 165–192.

Frank, W.M. (1977) The structure and energetics of the tropical cyclone II. Dynamics and energetics. *Monthly Weather Review*, 105, 1136–1160.

Gill, A.E. (1982) *Atmosphere–Ocean Dynamics*, 4th edition. New York: Academic Press.

Hogsett, W. and Zhang, D.-L. (2009) Numerical simulation of Hurricane Bonnie (1998). Part III: energetics. *Journal of the Atmospheric Sciences*, 66, 2678–2696.

Kilroy, G., Smith, R.K. and Montgomery, M.T. (2016) Why do model tropical cyclones grow progressively in size and decay in intensity after reaching maturity?. *Journal of the Atmospheric Sciences*, 73, 487–503.

Kurihara, Y. (1975) Budget analysis of a tropical cyclone simulated in an axisymmetric numerical model. *Journal of the Atmospheric Sciences*, 32, 25–59.

Mapes, B.E. and Zuidema, P. (1996) Radiative-dynamical consequences of dry tongues in the tropical troposphere. *Journal of the Atmospheric Sciences*, 53, 620–638.

McWilliams, J.C. (2011) *Fundamentals of Geophysical Fluid Dynamics*. Cambridge: Cambridge University Press.

Montgomery, M.T. and Smith, R.K. (2017a) Recent developments in the fluid dynamics of tropical cyclones. *Annual Review of Fluid Mechanics*, 49, 541–574. https://doi.org/10.1146/annurev-fluid-010816-060022.

Montgomery, M.T. and Smith, R.K. (2017b) On the applicability of linear, axisymmetric dynamics in intensifying and mature tropical cyclones. *Fluids*, 2, 69. https://doi.org/10.3390/fluids2040069.

Ooyama, K. (1969) Numerical simulation of the life-cycle of tropical cyclones. *Journal of the Atmospheric Sciences*, 26, 3–40.

Palmén, E. and Jordan, C.L. (1955) Note on the release of kinetic energy in tropical cyclones. *Tellus*, 7, 186–189.

Palmén, E. and Riehl, H. (1957) Budget of angular momentum and energy in tropical storms. *Journal of Meteorology*, 14, 150–159.

Peixoto, J.P. and Oort, A.H. (1992) *Physics of Climate*. New York: American Institute of Physics.

Smith, R.K. (2006) Accurate determination of a balanced axisymmetric vortex. *Tellus A*, 58, 98–103.

Smith, R.K. and Montgomery, M.T. (2016) Comments on "Nonlinear response of a tropical cyclone vortex to prescribed eyewall heating with and without surface friction in TCM4: Implications for tropical cyclone intensification." *Journal of the Atmospheric Sciences*, 73, 5101–5103.

Smith, R.K. and Vogl, S. (2008) A simple model of the hurricane boundary layer revisited. *Quarterly Journal of the Royal Meteorological Society*, 134, 337–351.

Smith, R.K., Montgomery, M.T. and Nguyen, S.V. (2009) Tropical cyclone spin up revisited. *Quarterly Journal of the Royal Meteorological Society*, 135, 1321–1335.

Tuleya, R.E. and Kurihara, Y. (1975) The energy and angular momentum budgets of a three-dimensional tropical cyclone model. *Journal of the Atmospheric Sciences*, 32, 287–301.

Wang, Y., Cui, X., Li, X., Zhang, W. and Huang, Y. (2016) Kinetic energy budget during the genesis period of Tropical Cyclone Durian (2001) in the South China Sea. *Monthly Weather Review*, 144, 2831–2854.

Zhang, J.A., Rogers, R.F., Nolan, D.S. and Marks, F.D. (2011) On the characteristic height scales of the hurricane boundary layer. *Monthly Weather Review*, 139, 2523–2535.

How to cite this article: Smith RK, Montgomery MT, Kilroy G. The generation of kinetic energy in tropical cyclones revisited. *Q J R Meteorol Soc.* 2018;144:2481–2490. https://doi.org/10.1002/qj.3332

APPENDIX: CALCULATION OF THE NET VERTICAL FORCE, *P*

The net vertical force per unit mass, P, defined in Equation 4 and used to construct Figure 5e,f was first calculated on the stretched model grid at the levels where thermodynamic quantities are defined. The vertical perturbation pressure gradient was determined by fitting a quadratic function to three successive levels, z_{i-1}, z_i and z_{i+1}, at which the perturbation pressure has values p'_{i-1}, p'_i and p'_{i+1}, respectively. Then

$$\left(\frac{\partial p'}{\partial z}\right)_i = \frac{(p'_{i+1} - p'_i)dz_i^2 - (p'_{i-1} - p'_i)dz_{i+1}^2}{dz_{i+1}dz_i(z_{i+1} - z_{i-1})}, \qquad \text{(A1)}$$

where $dz_i = z_i - z_{i-1}$.